Marine Geology 429 (2020) 106311

Contents lists available at ScienceDirect

Marine Geology

journal homepage: www.elsevier.com/locate/margo

The multi-decadal morphodynamic changes of the mouth bar in a mixed fluvial-tidal estuarine channel

Xiaoyan Zhou[a], Zhijun Dai[a,b,*], Xuefei Mei[a]

[a] State Key Laboratory of Estuarine and Coastal Research, East China Normal University, Shanghai 200062, China
[b] Laboratory for Marine Geology, Qingdao National Laboratory for Marine Science and Technology, Qingdao 266061, China

A R T I C L E I N F O

Keywords:
Morphodynamics
Inner-channel mouth Bar
Mixed fluvial-tidal estuary
Anthropogenic actions
ENSO events
Changjiang (Yangtze) estuary

A B S T R A C T

Inner-channel mouth bars (IMB) are common and vital geomorphological structures in estuaries that can efficiently promote the progradation of a fluvial delta. However, these significant structures face serious interferences by natural and human forces. This study mainly focuses on IMB deposited in the mixed fluvial-tidal dominated South Passage (SP) of the Changjiang Estuary between 1959 and 2018 to reveal how multidecadal morphodynamic variability in a mouth bar responds to natural forcing and human interferences. The results show that the volume of the IMB in the SP increased from 1128 × 10^6 m^3 in 1959 to 1636 × 10^6 m^3 in 1989 and then decreased to 462 × 10^6 m^3 in 2018. Meanwhile, the evolution of the IMB could be divided into five stages, the growing phase (1959 to 1979), which showed a 'V' shape, the partial adjustment phase (1999–2003), which showed a 'crest-dent' shape, the stable phase, which showed a flat shape (2004–2010), the partial adjustment phase (2011–2017), when Jiangyanan Shola inserted into the SP, and finally evolved into a flat shape in 2018. Fluvial water discharge and suspended sediment discharge (SSD) did not control the variation in the mouth bar. ENSO events were normally responsible for not only the periodic variations in the landward slope and the water depth of the crest of the IMB but also occasional extreme changes in the IMB. Moreover, local sandbar insertion, sediment from the seaside induced by strong tidal power and intensified engineering projects resulted in the continual shrinkage of the mouth bar by depositing more sediment at the mouth bar. Our work implies that understanding and governing this IMB will bring additional economic benefits to this fast-developing society, but the protection of this delicate estuarine geomorphology system should still receive great attention.

1. Introduction

A mouth bar, lying in the confluent regions between rivers or lakes and seas and serving as a crucial sedimentary unit of estuaries or deltas (Wright and Coleman, 1974; Allison, 1998; Anthony, 2015), has diverse configurations and locations depending on external forcings (Wright and Coleman, 1974). In the presence of moderate waves, larger mouth bars intend to be formed at a closer distance to the river mouth compared to the scenario without waves (Nardin et al., 2013). With respect to fluvial-dominated estuary, a wider mouth bar is situated near the entrance because of jet spreading, such as in the Changjiang Estuary (Ji-Yu et al., 1982) and the Mississippi Estuary (Leonardi et al., 2013). As for tidal-dominated case, a trifurcate mouth bar is generally detected inside the entrance of an estuary, such as in the Qiantang River Estuary (Qian and Wan, 1983) and Thames Estuary (Robinson, 1960). Otherwise, mouth bars are vital estuarine geomorphological units that are directly associated with distributary channel dynamics and deltaic development (Nardin and Fagherazzi, 2012; Leonardi et al., 2013). However, mouth bars are also natural barriers that seriously interfere with estuarine navigation due to their hump configuration in the longitudinal direction along a channel. Thereafter, how the morphodynamic changes in mouth bars vary with external forcing has received widespread attention around the world.

Some studies on mouth bar formation and evolution mechanisms have been conducted by numerical models, which can detect the impacts of an agent on a mouth bar or historical impacts aspects worldwide (Edmonds and Slingerl, 2007; Nardin and Fagherazzi, 2012; Esposito et al., 2013; Canestrelli et al., 2014; Luan et al., 2018). In a natural evolution process, Edmonds and Slingerl (2007) found that for distributary estuaries, the width, depth and length of a mouth bar in channel decrease nonlinearly with successive bifurcations, and the distance to the mouth bar is proportional to the jet momentum flux. Nardin and Fagherazzi (2012) adopted numerical experiments showing that waves affect the evolution of a mouth bar by modifying the river

* Corresponding author at: State Key Laboratory of Estuarine and Coastal Research, East China Normal University, Shanghai 200062, China.
E-mail address: zjdai@sklec.ecnu.edu.cn (Z. Dai).

https://doi.org/10.1016/j.margeo.2020.106311
Received 28 June 2020; Accepted 28 July 2020
Available online 03 August 2020
0025-3227/

jet's direction, bottom shear stress and changing the bottom friction. Esposito et al. (2013) noticed that alternating fine and coarse grain sediments during high and low flow conditions in a river-dominated mouth bar. Furthermore, Canestrelli et al. (2014) inferred that a stable jet would be more likely to form a mouth bar. As for anthropogenic interferences, Luan et al. (2018) analyzed morphodynamic impacts of the Deep Waterway Project (DWP) on the East Hengsha Shoal area during 1997–2013 through Delft 3D and topographic data. However, those studies were mainly focused on a microcosmic mechanism or a single impact factor of the changing process. Holistic analysis of the morphodynamic evolution of mouth bar coupling multi factors in most large estuaries around the world has received limited attention due to the serious shortage of long-term elevational data (Wal et al., 2002; Cuvilliez et al., 2009).

Complex natural forcing and anthropogenic interference will lead to dramatic changes of mouth area over a multiyear span from the geomorphological perspective (Moore, 1999; Wal et al., 2002; Blott et al., 2006; Nicholls and Tol, 2006; Reeve and Karunarathna, 2009; Cuvilliez et al., 2009). Most work has indicated that increasing ocean power, intrusion of saltwater, intensified storm surge activities, and sea level rise can all have significant effects on mouth bar evolution (Wright and Coleman, 1974; Shen et al., 1983; Reeve and Karunarathna, 2009). For instance, Wright and Coleman (1974) believed that salt-wedge intrusion was conducive to bed-load resuspension through crevasse channels with suspended loads, which tended to form a mouth bar. Shen et al. (1983) also indicated the point that saltwater intrusion would promote the deposition of a mouth bar in the Changjiang Estuary. Reeve and Karunarathna (2009) suggested that mouth bars in an estuary would maintain a stable state if there was an abundant sediment source from the external environment with sea level rise. However, the mouth bars of the Ribble Estuary, Gulf Coast and Bay of Bengal have all experienced long-term shrinkage due to channel dredging or the construction of structures (Moore, 1999; Wal et al., 2002; Cuvilliez et al., 2009). Furthermore, Yang et al. (2005) and Syvitski et al. (2009) stated that dam construction leads to sediment starvation, which can also cause erosion of the delta front and mouth bar area. Dai et al. (2013) noticed that the mouth bar still existed in an estuary, even though the construction of the Three Gorges Dam (TGD) in 2003, the largest dam in the world, intercepted tons of sediment load that was normally transported to the East China Sea. Anthony (2015) and Liu et al. (2017) suggested that dam construction, commercial sand mining and groundwater extraction caused vulnerability of the Mekong mouth bar area. Nonetheless, Gugliotta and Saito (2019) discovered that the mouth bars associated with the Colorado Delta still maintain a significant natural state, although major human-induced changes have occurred. A recent study indicated an erosion-deposition pattern of the entire Changjiang Estuary and revealed that obvious deposition occurred with diminished fluvial sediment supply because of water regulation, caused by impoundment of the TGD, and sediment from the sea (Zhu et al., 2020). Therefore, the decisive factors that control the geomorphology status of a mouth bar and the contributions from natural and human interferences remain a conundrum, even though many studies have been conducted in recent years, especially in the mega-estuary in China, the Changjiang (Yangtze) Estuary.

The Changjiang basin has supported millions of lives in China, and a major delta system was built that extends for more than 50,000 km^2, which represents the largest estuary in China (Chen et al., 2001). There are four channels connected to the river and sea (Fig. 1a, b). Due to the plentiful sediment supply (433 mt/year during 1950–2000) from the Changjiang River (http://www.cjh.com.cn/), an enormous mouth bar system has been silted with depths less than 10 m and extension lengths exceeding 40 km along each channel (Fig. 1b) (Ji-Yu et al., 1982). Descriptions of the basic characteristics of the mouth bar in the Changjiang Estuary have been made since the 1950s (Ji-Yu et al., 1982; Milliman et al., 1985). According to Ji-Yu et al. (1982), the system can be divided into shoal and inner-channel mouth bar (IMB), which is

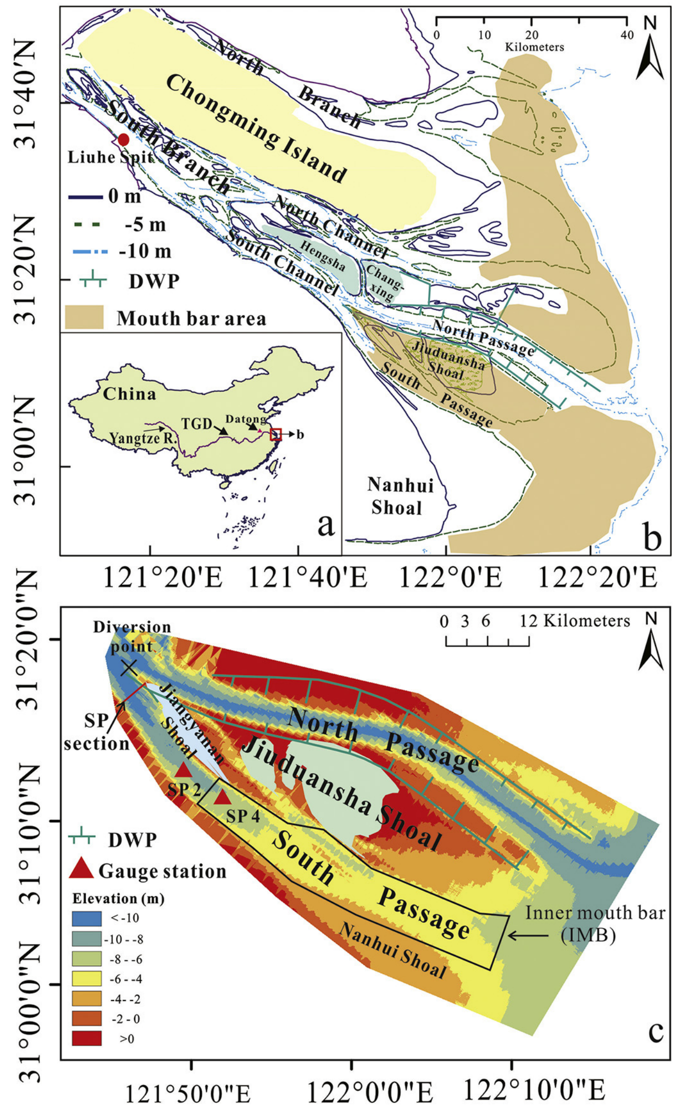

Fig. 1. (a) Map of Changjiang with its location in relation to China and the location of the Three Gorges Dam and Datong gauge station; (b) Changjiang Estuary with the bathymetry in 2013 with 0, −5 and −10 m isobaths. Dash area in orange showed the whole mouth bar region; (c) Bathymetry map of the South Passage with the bathymetry in 2018 with gauge stations for measuring ebb flow coefficient (SP2 and SP4), SP section for measuring the ebb flow diversion ratio of the SP and the Deep Waterway Project (DWP).

distinguished by the water depth of −5 m. Shoal mouth bar is usually above the −5 m isobath and IMB is limited between −5 m to −10 m. In comparisons with IBM, shoal mouth bar normally gets more study because this structure is usually above the water and easy to depict (Wei et al., 2019). IMB is essential part for estuary progradation and shipping commercial. However, little information is available related to quantitative analyses of the decadal morphological changes in the IMB under the context of anthropogenic interferences and natural forcing (Dai et al., 2013).

Concerning the complex characteristics of each entrance, different mechanisms play leading roles in the evolution of the mouth bars in the Changjiang Estuary. For shoal mouth bar, proximal engineering projects and natural forcing can both alter its local geomorphology in a long time scale, like Jiuduansha Shoal and Nanhui Shoal, which locate at both side of the SP (Wei et al., 2019; Zhu et al., 2019b). For IMB, the NB's mouth bar occupies almost the whole waterway and shows a silting trend with elongation under a water depth of −5 m, even though the suspended sediment discharge (SSD) from upstream declined obviously from 1958 to 2013 (Dai et al., 2013; Dai et al., 2016). Similarly, the IMB area along the NC exhibited erosion in the upper reach but deposition in the lower reach during 1880 to 2013 (Mei et al., 2018a). For the NP, DWP is responsible for the constant water depth of 12.5 m; thus, the mouth bar in this entrance has not varied much, even though intensified human activities have occurred (Dai et al., 2013). Completely different from the NP, the SP is not only a major conduit for Changjiang riverine sediment and flux (Milliman et al., 1985), but also a vital channel for vessels reaching Shanghai Port with 71.1% occupation of the entire amount of vessels that passed through the Changjiang Estuary (https://www.cjkhd.com/news1/0/960). Average flow rate in the SP during flood and dry season in 2018 were 0.74 m/s and 1.02 m/s, respectively, when monthly average fluvial discharge supply were respectively 15,887 m^3/s and 42,456 m^3/s, indicating that the IMB in the SP is affected by both tidal and fluvial forces. Meanwhile the SP channel is rarely affected by the wave forcing owned to a weak wave influence of 0.4 m wave height near the entrance of the SP (Chen et al., 1999; Wei et al., 2019). Therefore, the SP offering a typical case to determine whether and how the natural processes of the IMB of a mixed estuary have been impacted by natural forcing with a mixture of anthropogenic inferences over nearly 60 years. Although Yang et al. (2001) studied the response of bed level to water discharge and coastal storm of the IMB in the SP between 1988–1990, the IMB's evolution process in a multi-decadal timescale in the SP under coupling factors is still missing. Therefore, the aim of this study is 1) to discern the factor controlling the evolution process of the IMB and 2) to diagnose the growing pattern of the IMB. It is very significant for hydraulic engineers and policy-makers to recognize the factors that will impact IMB morphodynamics and to make appropriate decisions to address similar mouth bar evolution processes in other large estuaries of the world.

2. Materials and methods

2.1. Data and materials

Five sets of data are utilized in this study. The first group of data is the bathymetric points for the SP (Table 1). Digital water depths of the SP during the flood seasons in 1959, 1979, and 1989 were digitized from nautical chart with ± 0.1 m vertical accuracy, which were recorded by the Deso-17 echo-sounder (Dai et al., 2016). During flood (August) and dry (February) season from 1999 to 2018 were measured via single-frequency sounding technology and multibeam echo sounder from Konsberg Maritime, which both owned vertical error of 0.1 m and positioning error of 1 m. These water depths were measured along cross-sections with an interval of 1 km and only covered the SP and its adjacent sandbar. The water depths were transferred to the Beijing 54 coordinates system and calibrated to the "Wusong Datum" in ArcGIS 10.2. These data were acquired from the Changjiang Estuary Waterway Administration Bureau (CJWAB), Ministry of Transportation of China.

Table 1
Bathymetric data covering CMB of South passage, by CJWAB.

Year	February	May	August	Scale
1959			√	
1979			√	
1989			√	
1999	√		√	1:25000
2000	√		√	1:25000
2001	√			1:25000
2002	√		√	1:25000
2003	√		√	1:25000
2004	√		√	1:10000
2005	√		√	1:10000
2006	√		√	1:10000
2007	√		√	1:10000
2008		√		1:10000
2009		√		1:10000
2010	√		√	1:10000
2011	√		√	1:10000
2012	√		√	1:10000
2013	√		√	1:10000
2014		√	√	1:10000
2015		√	√	1:10000
2016		√	√	1:10000
2017		√	√	1:10000
2018		√		1:10000

The second set of data is the ebb flow diversion of the SP. These data from 1964–2013 were collected by the CJWAB. This indicator can be defined as the rate between the ebb tidal volume (V_{SP}) through a specific section of the SP and its sum through both the NP and SP ($V_{NP} + V_{SP}$). The ratio can be calculated as follows:

$$E_{SP} = \frac{V_{SP}}{V_{NP} + V_{SP}} \tag{1}$$

The third set of data is the coefficient of flow dominance (See Table 2), which was put forward by Simmons (1955). Several measurement points are set in the vertical direction to obtain the current speed at different depths, and then a speed variation process portrait can be used to calculate the coefficient, which is the rate between the area of flood tide velocity (E) and the sum of the area of flood (F) and ebb tide velocity. The coefficient can be calculated as follows:

$$P = \frac{E}{E + F} \times 100\% \tag{2}$$

when $P > 50\%$, it implies that the location of the hydrographic station is dominated by ebb currents; otherwise, it dominated by tidal currents. In this article, data from two gauge stations were analyzed (gauge stations are shown in Fig. 1c).

The fourth set of data included the yearly and monthly water discharge and suspended sediment flux during 1959–2018 at the Datong Gauge Station (Fig. 1c), which were collected by the Bulletin of China River Sediment.

The fifth data point was the half-yearly ENSO index from 1959 to 2018 in the Niño 3.4 region (5°N ~ 5°S, 120° ~ 170°W), which was collected by a global climate observing system (http://www.esrl.noaa.gov/psd/gcos_wgsp/Timeseries/Nino34/index.html). The ENSO index was calculated from the sea surface temperature (SST) by National Oceanic and Atmospheric Administration (NOAA) in this region. An El Niño event is defined as a period of 5 consecutive months with the SST exceeds 0.5 °C of the average, and inversely, La Niña is a phase when the SST is 0.5 °C below the average for 5 consecutive months. Ninety-five percent and 5% of the ENSO index can be set as thresholds to define an extreme event.

2.2. Methods

Each digital water spots of the SP can be interpolated into a digital evaluation model (DEM) with a 50 × 50 m grid resolution by the triangular irregular network (TIN) interpolation method, which is widely adopted in bathymetric analysis (Andes and Cox, 2017). It is efficient to analyze geomorphological changes in estuaries with a DEM (Jaffe et al., 2007; Falcão et al., 2013).

Volume calculation and slope extraction are both performed in ArcGIS 10.2. Since the area with steeper slope (Fig. 2a) was coincided with the −5 m isobath and the slope at the −10 m depth was unobvious, the −10 m and −5 m isobaths were set as the upper and lower boundary of the IMB, respectively (Ji-Yu et al., 1982). Our study focused on the mouth bar in the SP, thus that part locating outside the SP was ignored in this study. According to the boundaries, landward slope (LWS) and seaward slope (SWS) were extracted from the two cross sections and their averaged values were defined as LWS and SWS (Fig. 2a). The volume of the mouth bar in the SP was bounded by the −5 m isobaths of the Jiuduansha Shoal to the north and the −5 m isobaths of the Nanhui Shoal to the south (Fig. 2b). The volume data

Table 2
Obtained coefficient of the ebb flow dominance.

Gauge station	Coordinate	Surveyed periods
SP 2	121.85°E, 31.19°N	Feb. Aug.2002, Feb. Aug.2005, Jan. 2007, Jan. Aug. 2010, Feb. 2011, Feb. Aug. 2012.
SP 4	122.05°E, 31.07°N	Aug. 2007, Aug. 2011, Aug. 2015.

during Aug. 2001 were not collected, so only the volume in Feb. 2001 was calculated to be 227 × 10^6 m^3, and this information is not shown in Fig. 8. Parameters representing the mouth bar configuration, including the seaward and landward slopes, were calculated as follows based on the previous TIN interpolation (Fig. 2):

$$\partial = \tan^{-1}\sqrt{\frac{Elevation}{Distance}} \tag{3}$$

∂ is the slope of the two water depth points. After the DEM was built, all ∂s can be calculated among these depth points. The average ∂s was calculated both landward and seaward of the mouth bar in the SP as landward and seaward slopes, respectively. Additionally, thalwegs were extracted by the deepest points at each section, representing profiles of the IMB and crests were defined as the shallowest points along the thalweg.

To evaluate the extreme high (low) events, setting a 75th (25th) percentile threshold of the daily SSD value is set according to Intergovernmental Panel on Climate Change (IPCC) Fourth Assessment Report (Bonsal et al., 2001; Dai et al., 2016).

Wavelet analysis was applied in this study to examine whether a periodic fluctuation occurred in the morphodynamic configuration of the mouth bar, the landward slope series or the depth series of the crest of the mouth bar in the SP. This analysis method has been utilized frequently in recent years (Torrence and Compo, 1998; Dai et al., 2019). The following expression shows a continuous wavelet transform:

$$\begin{aligned} W(a,b) &= \langle x(t), \varphi_{a,b}(t) \rangle \\ &= \int_{-\infty}^{+\infty} x(t)\varphi_{a,b}^{*}(t)dt \frac{1}{\sqrt{a}} \int_{-\infty}^{+\infty} x(t)\varphi^{*}\left(\frac{t-b}{a}\right)dt \ \ a, b\epsilon R, \ a \neq 0 \end{aligned} \tag{4}$$

In this formula, x(t) is a value series of the parameter that needs to

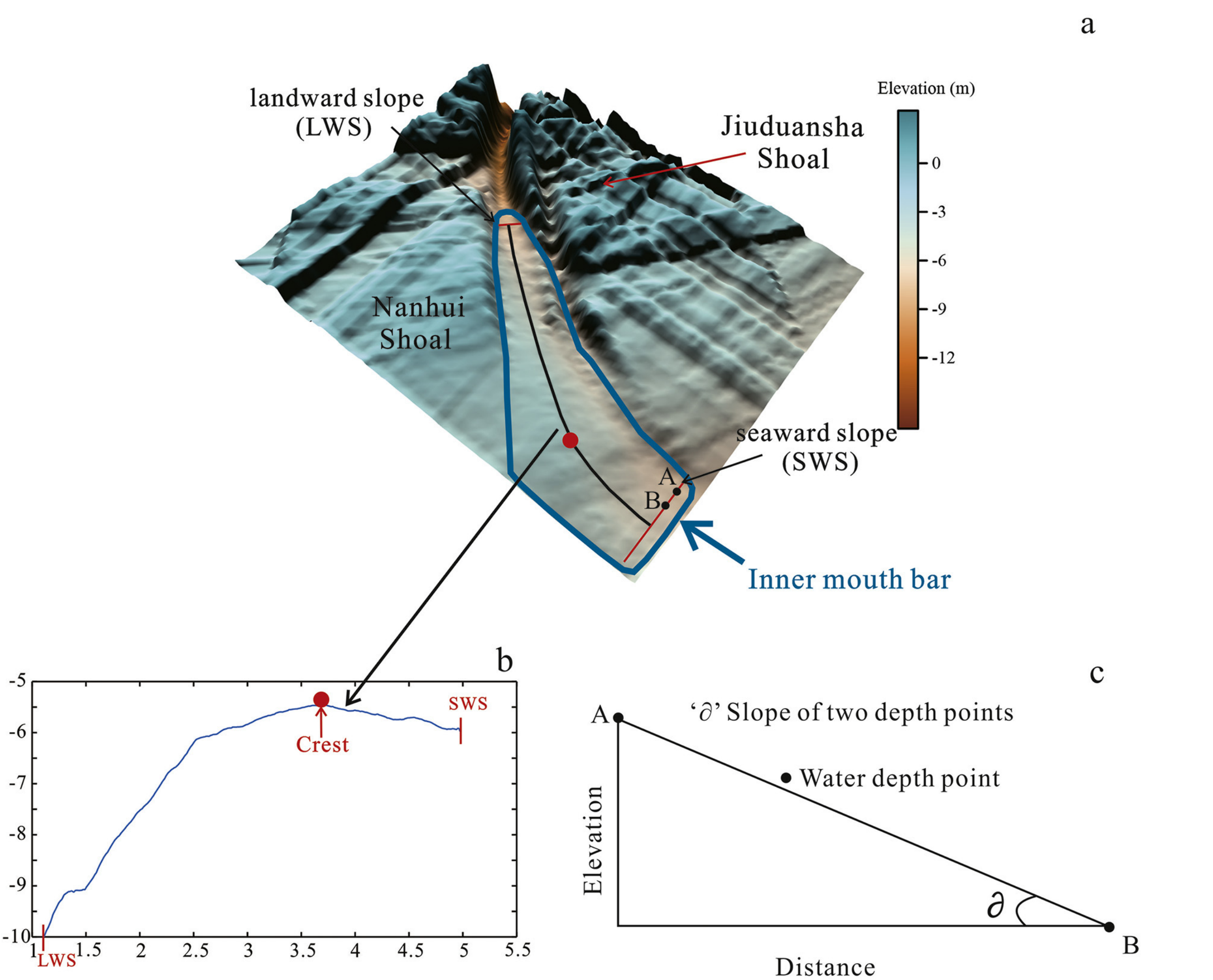

Fig. 2. (a) Three-dimensional sketch of inner mouth bar in the in the South Passage with the bathymetry in 2018, showing inner mouth bar's profile (blue solid line), thalweg (black solid line), landward slope (LWS, red solid line in the upper part) and seaward slope (SWS, red solid line in the lower part); (b) The elevation of thalweg extracting from (a); (c) Sketch diagram showing the calculation of slope, where A and B represented two adjacent grids. (For interpretation of the references to colour in this figure legend, the reader is referred to the web version of this article.)

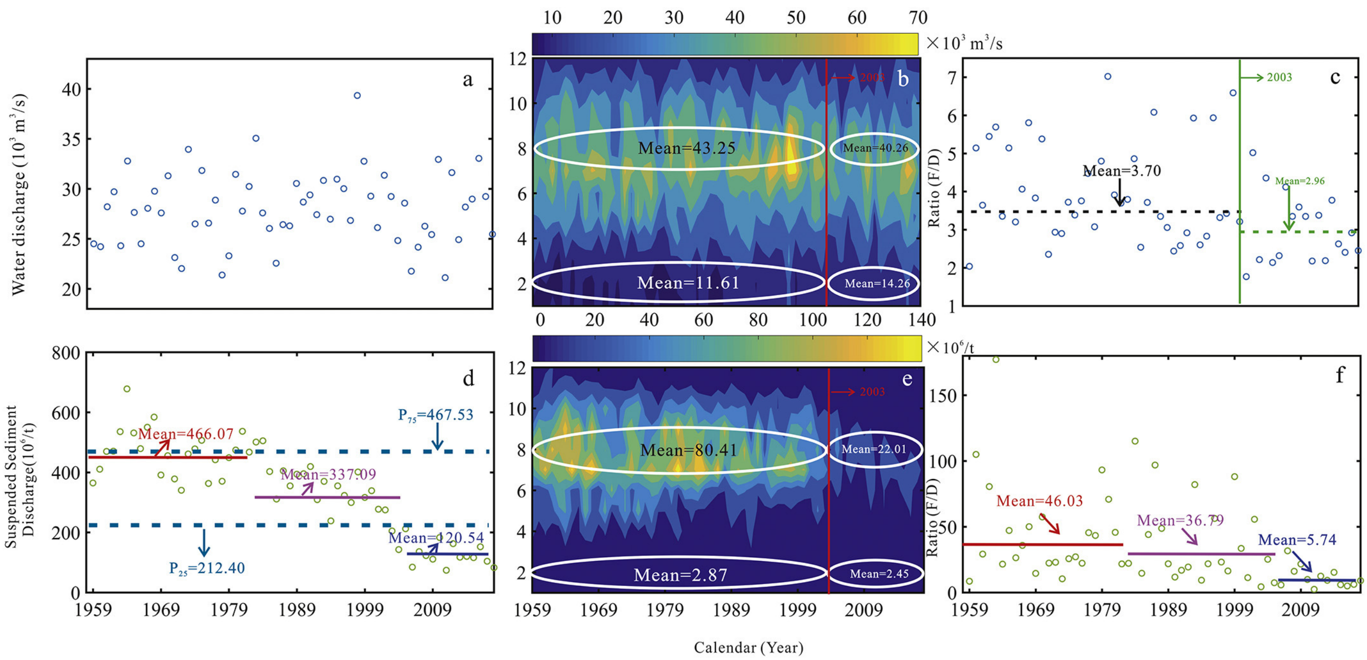

Fig. 3. Changes in runoff and suspended sediment discharge at Datong gauge station, with (a) yearly water discharge during 1959–2018; (b) Monthly water discharge during 1959–2018 (c) The ratio between flood and dry season of the water discharge; (d) Yearly suspended sediment discharge during 1959–2018; (e) (b) Monthly suspended sediment discharge during 1959–2018 (c) The ratio between flood and dry season of the suspended sediment discharge.

be detected to determine whether periodic fluctuation exists, for example, the landward slopes and depth of the mouth bar; a and t represent the scale and time parameters, respectively. φ(t) is the wavelet basis function, and $\varphi^*(t)$ represents the complex conjugate of the wavelet coefficient.

This study adopted the complex Morlet wavelet as the wavelet basis function, which is shown as follows:

$$\varphi(t) = \frac{1}{\sqrt{\pi f_b}} e^{i2\pi f_c t - (t^2/f_b)} \tag{5}$$

where f_c indicates the central frequency of the mother wavelet and f_b represents the bandwidth.

3. Results

3.1. Variations in runoff and suspended sediment discharge (SSD) from upstream

Yearly water discharge changed little between 1959 and 2018 (Fig. 3a) yet the monthly value exhibited distinct seasonal patterns (Fig. 3b). The water discharge in Feb. increased from 11.61 m^3/s during 1959 to 2002 to 14.26 × 10^3 m^3/s during 2003 to 2018, and in August, the value decreased from 43.25 × 10^3 m^3/s (1959 to 2002) to 40.26 × 10^3 m^3/s (2003 to 2018), demonstrating no flood in the flood season and no drought in the dry season; thus, 2003, was set as a threshold (Fig. 3b). During the period of 1959 to 2002, the ratio between flood and dry season of water discharge was 3.7 (Fig. 3c). However, the ratio decreased to 2.96 during the period of 2003 to 2018 (Fig. 3c).

Different from the relatively stable value of water discharge, the yearly SSD exhibited three variation phases according to the 'threshold method' mentioned in Chapter 2.2, which were 1959 to 1982, 1983 to 2005 and 2006 to 2018 (Fig. 3d). The average SSD was 466.07 × 10^6 t, 337.09 × 10^6 t and 120.54 × 10^6 t at the three stages, respectively (Fig. 3d). The seasonal pattern also varied obviously: before 2003, the SSD in the flood season was 80.41 × 10^6 t, and after 2003, it decreased to 22.01 × 10^6 t, which was a decrease of approximately 44 times (Fig. 3d, e). For the dry season, the value decreased from 2.87 to 2.45 × 10^6 t; thus, 2003 was set as a threshold (Fig. 3e). The SSD in both the flood and dry seasons decreased sharply after 2003 (Fig. 3f).

3.2. Changes in the configuration of the inner mouth bar

The IMB of the SP is arcuate in shape with a length of 60.95 km on average, and the longitudinal length increased by 12.15 km from 1959 to the 2010s (Fig. 4). Meanwhile, the configuration of the IMB exhibited an inherent evolution pattern during the observation period. Between 1959 and 1979, the IMB configuration was mainly presented as a 'V' shape (the blue and orange dotted lines in Fig. 4a), and in 1989, the IMB shifted to a flat shape without an obvious crest (solid yellow line in Fig. 4a). However, during 1999 and 2003, the inner mouth bar exhibited an inverted 'W' shape, which showed two crests with a dent between them during 1999 and 2003 (Fig. 4b). Between 2004 and 2010, crests disappeared and the dent elevated, making the IMB appear as a 'flat' shape (Fig. 4c). At this period, the configuration remained smooth with a symmetry shape. During 2011 and 2017, however, there appeared an obvious crest again with a dent, becoming asymmetrical (Fig. 4d and e). In 2018, the crest and the dent tended disappear and a flat pattern showed again. Furthermore, this evolution from a 'crest-dent' shape into a 'flat' shape was also observed in dry season (Fig. 4g–l), when the crest remained longer (Fig. 4j and k). In addition, with top disappearances, the single crest moved downstream by approximately 27.81 km and was elevated from 1959 to 2018 by approximately 1.24 m, averagely (Table 3).

Moreover, the landward slope of the mouth bar decreased while the seaward slope increased in both the flood and dry seasons during these years (Fig. 5a and b). The landward slope was always almost two times larger than the seaward slope between 1999 and 2018 (Fig. 5a). For the landward slope in the flood season, the decreasing rates were 2/1000 per year (Fig. 5a) and 1.5/1000 per year in the dry season (Fig. 5b). For the seaward slope, the increasing rates were 0.7/1000 (Fig. 5a) and 1.3/1000 (Fig. 5b) per year in the flood and dry seasons, respectively. The landward slope has wider oscillation ranges of 0.03° to 0.13° and 0.03° to 0.12° in the flood and dry seasons, respectively, even though

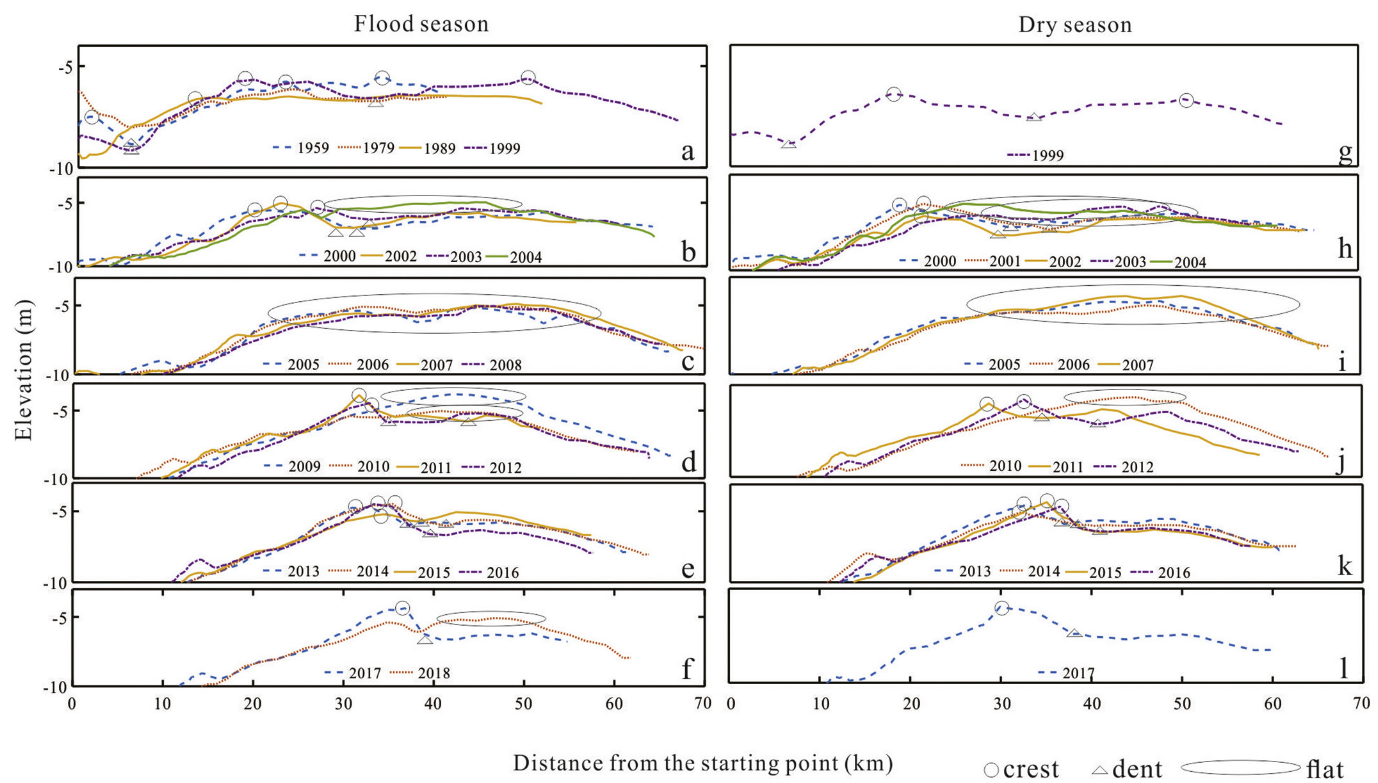

Fig. 4. Changes in thalwegs of the inner mouth bar during 1959–2018. The starting point of the horizontal axis is the diversion point of the NP and SP. (a–f) Thalwegs elevation of the IMB in flood season during 1959–2018; (g–l) Thalwegs elevation of the IMB in dry season in 1999–2017.

Table 3
Crests' information during 1959– 2018.

		Distance from the starting point (km)	Elevation (m)	Average distance (km)	Average elevation (m)
1959	Upper part	1.65	−7.69		
	Middle part	22.74	−5.75		
	Lower part	33.67	−5.50	19.35	−6.31
1979	Upper part	0.45	−6.29		
	Lower part	24.24	−6.15	12.345	−6.22
1989	Only one	22.89	−6.23	22.89	−6.23
1999	Upper part	19.60	−5.63		
	Lower part	49.98	−5.56	34.79	−5.60
2018	Only one	47.16	−5.07	47.16	−5.07

there were small oscillations in the seaward slope (Fig. 5a and b). A continuous wavelet transform is applied to these slopes to detect if any regular fluctuations exist. Fig. 5c and d illustrates that a 2-year period passed a red noise examination with a significance level of 0.1. The result implied that the landward slope had an evident cycle of 2–4 years.

3.3. Changes in crests of the inner mouth bar

The crest of the IMB is a stable product of riverine and marine forcings and sediment accumulation, which can reflect external hydrological conditions and morphodynamic changes in the IMB (Shen et al., 1983). The mean elevation of the mouth bar crest was 4.88 m during the flood season and 4.72 m during the dry season between 1959 and 2018. Moreover, the top of the IMB became shallower during this period with an average elevated height of 1.24 m from 1959 to 2018 (Table 3). In addition, although the TGD's operation in 2003 intercepted tons of sediment from upstream, the crest still exhibited a deposition trend during 2003 to 2018 (Fig. 6a and b). Furthermore, wavelet analysis was also performed in Fig. 7a and b to recognize whether an oscillation period existed in the crest depth series. The corresponding results implied that the crest depth series had an evident cycle of 2 years (Fig. 7).

In addition to the water depth of these tops, their distances from the diversion point (Fig. 1c) were calculated to reflect the relative strength between runoff and tides. In average, the crest was moved 27.81 km downstream between 1959 and 2018 (Fig. 6c and d). Meanwhile, during the flood seasons of 1989, 2006, 2011 and 2016, the top suddenly moved 23.58 km, 12.07 km, 10.89 km and 9.96 km upstream from the crest location in the previous year, respectively. In 1999, the top moved 48.87 km downstream from the former year's location, which was the farthest crest from the diversion point among these years. In the dry season, the top abruptly moved 23.75 km downstream in 2003 and moved 17.16 km upstream in 2011 compared with the crest's location in the former year (Fig. 6d).

3.4. Volume variations of the inner mouth bar

The IMB's volume increased from 1128 × 10^6 m^3 to 1636 × 10^6 m^3 from 1959–1989 and then decreased to 462 × 10^6 m^3 in 2018 (Fig. 8a and b). Since 1999, the average yearly volume increased at a rate of 12.06 m^3/year until 2018. However, this increasing rate began to slow in 2017. Since volume data in the dry season from 1959 to 1989 and 2018 were lacking, volume data from only 1999 to 2017 were analyzed in both the flood and dry seasons. The results show that the volume of the IMB increased from 224 × 10^6 m^3 to 462 × 10^6 m^3 in the flood season from 1999 to 2017, and in the dry season, the value changed from 256 × 10^6 m^3 to 459 × 10^6 m^3 (Fig. 8c). Taken together, these results indicate that the mouth bar volume increased by 106.53% from 1999 during the flood season and 79.43% during the dry season. Additionally, the increasing rate in the flood season was 15 × 10^6 m^3/year, which is slightly larger than the rate in the dry season, which was 11 × 10^6 m^3/year (Fig. 8c). Over a relatively long-term period of

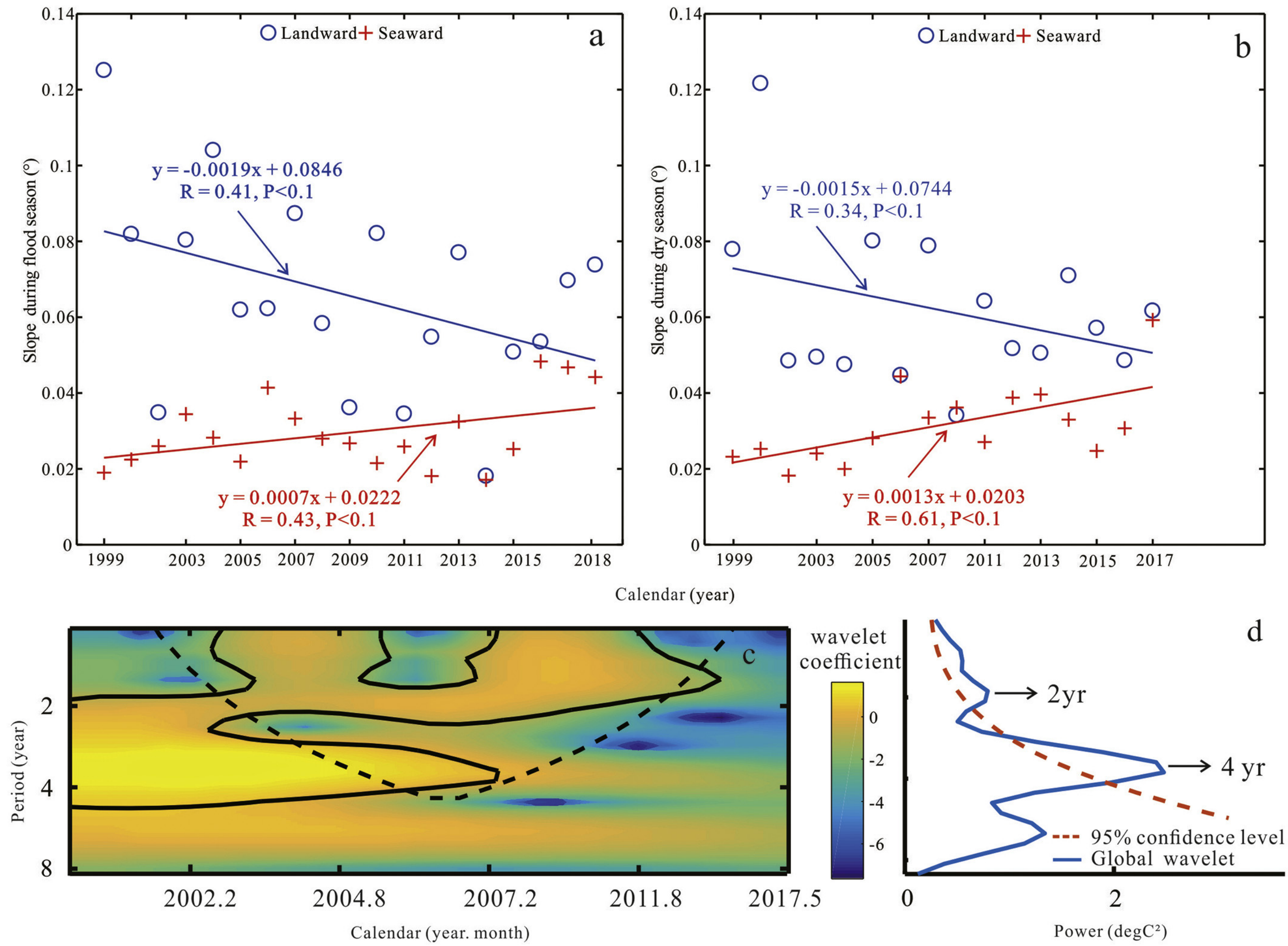

Fig. 5. (a) Landward slope and seaward slope of the inner mouth bar during flood season; (b) Landward slope and seaward slope of the inner mouth bar during during dry season; c) Wavelet analysis of the landward slope of the inner mouth bar between surveys which are the contoured coefficient and global wavelet coefficient, respectively; (d) Result of the red noise test of the global Wavelet Coefficient. Blue spike passed over the 95% confidence level inferring the effective period. (For interpretation of the references to colour in this figure legend, the reader is referred to the web version of this article.)

nearly 20 years, the mouth bar's volume did not exhibit an obvious seasonal pattern.

4. Discussion

4.1. Impacts from upstream areas with TGD interference

The formation and evolution of a mouth bar are sensitive to runoff, sediment discharge, tides, waves and winds (Blott et al., 2006; Nicholls and Tol, 2006; Reeve and Karunarathna, 2009; Nardin and Fagherazzi, 2012). Although some deltas experience shoreline retreat and channel erosion in response to a shrinking mouth bar (Syvitski et al., 2009; Anthony, 2015; Liu et al., 2017), the Pearson coefficients (PC) of water discharge with the volume of the IMB in the SP were −0.08 (Fig. 9). Except three volumes in 1959, 1979 and 1989, which were much beyond the mean volume, the PC of SSD, which were smaller than 500 × 10^6 t with volume of the IMB was −0.63, inferring that although the SSD had a stronger relationship with the volume than water discharge, they both were not controlling factors of the IMB.

Meanwhile, the configuration and location of the mouth bar rarely changed during both the flood and dry seasons in the same year, although the water discharge from upstream areas exhibited an obvious seasonal pattern, and the discharge was almost 4 times larger in the flood season than that in the dry season (Fig. 3c and f). In addition, the TGD caused a drastic decline in suspended sediment after 2003 (Fig. 3d), which did not lead to erosion or degradation of the IMB (Fig. 8b). Thus, it can be concluded that the IMB of a mixed fluvial-tidal estuary will not obviously respond even though the fluvial conditions from upstream have exhibited distinct changes. The evolution process of the IMB in the SP can have other controlling agents instead of fluvial water discharge and SSD. Furthermore, a positive connection between mouth bar erosion and SSD decline does not exist in other large estuaries, especially this mega-estuary, which has a complicated evolution mechanism (Besset et al., 2019, Gugliotta and Saito, 2019).

4.2. Impacts from regional tidal forcing

Fluvial sediment and adjacent morphological units are not the only sources of material for an estuary mouth bar, longshore currents, wave and tide transportation also occur during the long-term formation process and sediment is transported from the outlet to the IMB (Rahman et al., 2011; Anthony, 2015; Wilson and Goodbred Jr., 2015; Dai et al., 2016; Boudet et al., 2017; Hoitink et al., 2017; Hu et al., 2017). Compared to the tide and fluvial forcings, wave forcing outside the SP entrance only generated a wave height of 0.4 m, which has limited influence on the mouth bar in the channel (Wei et al., 2019). Therefore, the wave forcing hardly affect the IMB's evolution process. Meanwhile, variations in the configuration and location of the IMB could have a

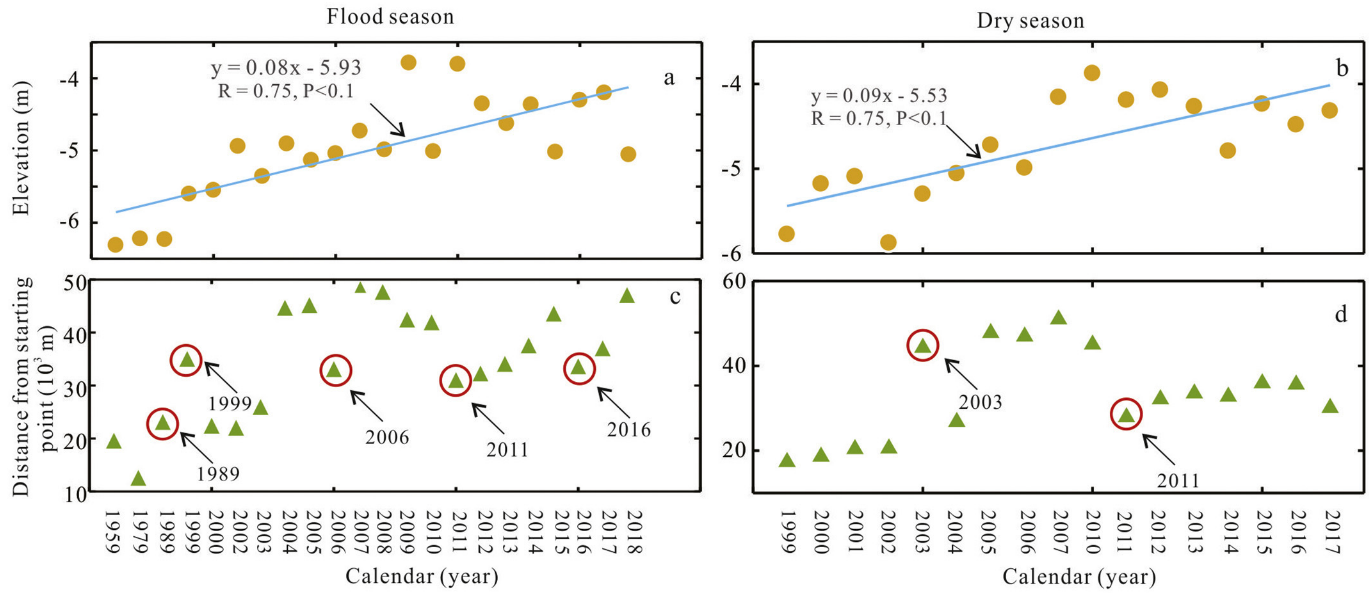

Fig. 6. Elevation and distance from the starting point of the crest of the mouth bar; a) and b) show the crest water depths in flood and dry seasons; c) and d) show the distance from the starting point of the crest. The starting point of the vertical axis indicates the diversion point of the NP and SP (black cross in Fig. 1c). Red circles show the year of sudden changes of the mouth bar. (For interpretation of the references to colour in this figure legend, the reader is referred to the web version of this article.)

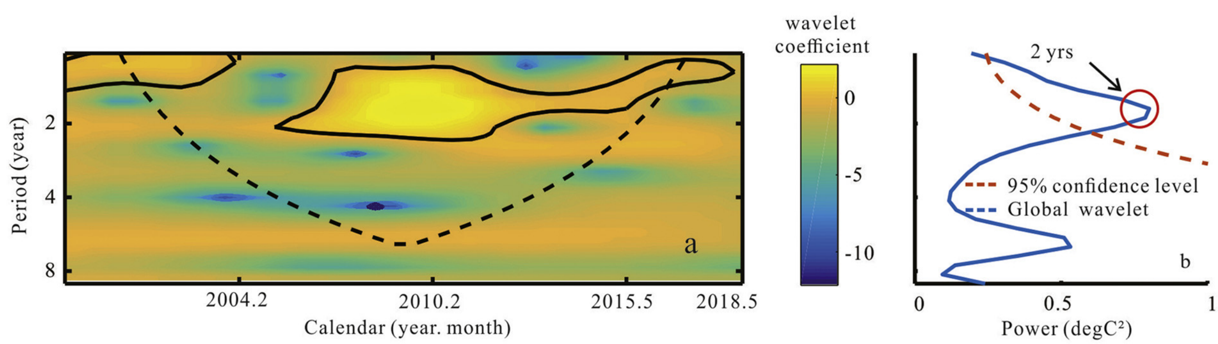

Fig. 7. (a) Wavelet analysis of the crest's elevation of the inner mouth bar between surveys which are the contoured coefficient and global wavelet coefficient, respectively; (b) Result of the red noise test of the global Wavelet Coefficient. Blue spike passed over the 95% confidence level inferring the effective period. (For interpretation of the references to colour in this figure legend, the reader is referred to the web version of this article.)

cycling period, such as the lunar perigee of 8.85 year or lunar nodal cycle of 18.61 year due to impacts from long-term periodic tidal cycles (Cartwright, 1974; Wood, 2001; Haigh et al., 2011). Since the continuous topological data of this study only covered 20 years from 1999 to 2018, concentration was put on the IMB's short periodical variation.

Some work has indicated that the water depth at the mouth bar region tends to decrease (shallowing) due to landward sediment movement by flood-dominant tidal forces (Swenson et al., 2005; Gugliotta and Saito, 2019). The coefficient of ebb flow in the SP was used to analyze the contributions of tides to the Changjiang Estuary during these years. Two gauge stations (SP2 and SP4 in Fig. 1) in the SP both measured a decreasing coefficient in almost every stage (Table 4) since 1999 (except in the dry seasons of some years), suggesting an increasing tidal forcing that carried sediment from seaward areas that was deposited on the seaward side of the mouth bar, steepening the seaward slope (Fig. 5a and b) and elevating the depth of the crest so that the crest moved downstream (Fig. 6). Even if crest's elevation 2011 exhibited a decreasing trend after 2011, the whole IMB's size still enlarged (Fig. 8b) owing to the increasing tidal forcing (Table 4). Moreover, the appearance and development of a flood tidal channel (Fig. 1c, Fig. 12b, c, d and e) also confirms this scenario.

The Colorado River Mouth, Ebro Estuary and Rhône delta have confronted similar circumstances in which seaward forcing became relatively stronger, reworking deltas and leading to a deposition trend in the channel or prodeltaic lobes (Sanchez-Arcilla et al., 1998; Sabatier et al., 2006; Sabatier et al., 2009; Zamora et al., 2013). For the Damietta Spit in the Nile Delta, although serious erosion occurred along promontories after the Aswan Dam began operation, considerable sediment was swept from the outer margin into the river mouths by waves, building the spit (Frihy and Lawrence, 2004). Stronger forcing from seaside triggering a 'source-shift' from riverine to sea.

With the increasing power from both the land and sea, the mouth bar was squeezed and its length significantly decreased in the last three stages (Fig. 12b, c and d), except for when a dredging project was carried out in 2013, which subsequently led to a stable water depth of the mouth bar. An increased sediment load from the sea resulted in crest deposition at the seaside and shortened the length of the mouth bar. The ebb flow diversion ratio of the SP continued to increase (Fig. 11a), but sediment from upstream decreased, which decreased the landward slope (Fig. 5a and b) since less sediment could build up. The only top was pushed away and moved to a shallower depth by the sediment from the seaside, which was caused by a stronger force.

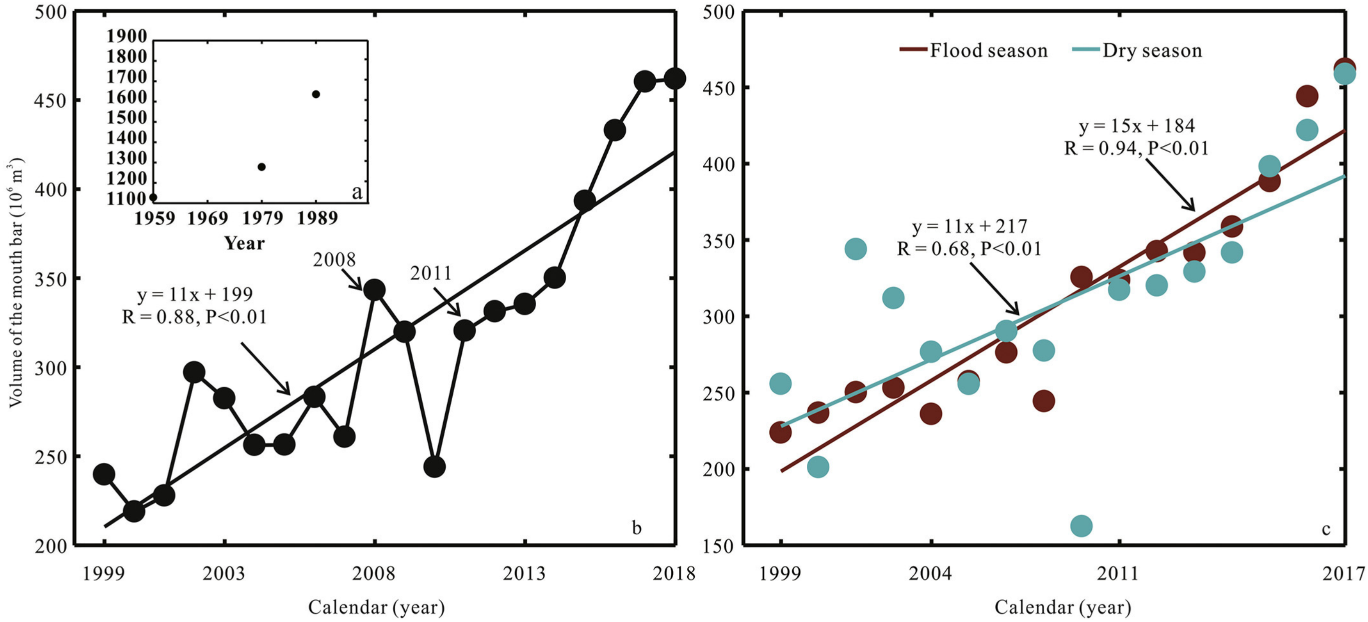

Fig. 8. Volume of the mouth bar in the flood and dry seasons during 1959–2018. The average yearly volume of the mouth bar in (a) 1959 to 1989 and (b) 1999 to 2018 (black lines and dots); (c)Volume of the inner mouth bar from 1999 to 2017, where the brun line and dots represents the flood season and the blue line and dots represents the dry season. (For interpretation of the references to colour in this figure legend, the reader is referred to the web version of this article.)

4.3. Effects of ENSO events

Dai et al. (2019) inferred that solar and lunar periodic motions were important factors that had impact on the world's hydrological and geomorphology process of large rivers and their estuaries. Regionally, Zhu et al. (2019b) found that ENSO events were the main agent of plum rains in the Changjiang Delta with a 3-year cycle, which suggests a potential linkage between macrolevel climate changes and regional variation. As shown in Figs. 5c, d and 7, nearly 2 to 4 years periodic variations in the landward slope and crest depth of the mouth bar can be detected, which coincided with ENSO episodes according to the results from wavelet analysis. On the other hand, different indexes of the mouth bar responded to the ENSO signals to different extents (Fig. 6c and d, Fig. 8a). A comparison was made between ENSO signals and

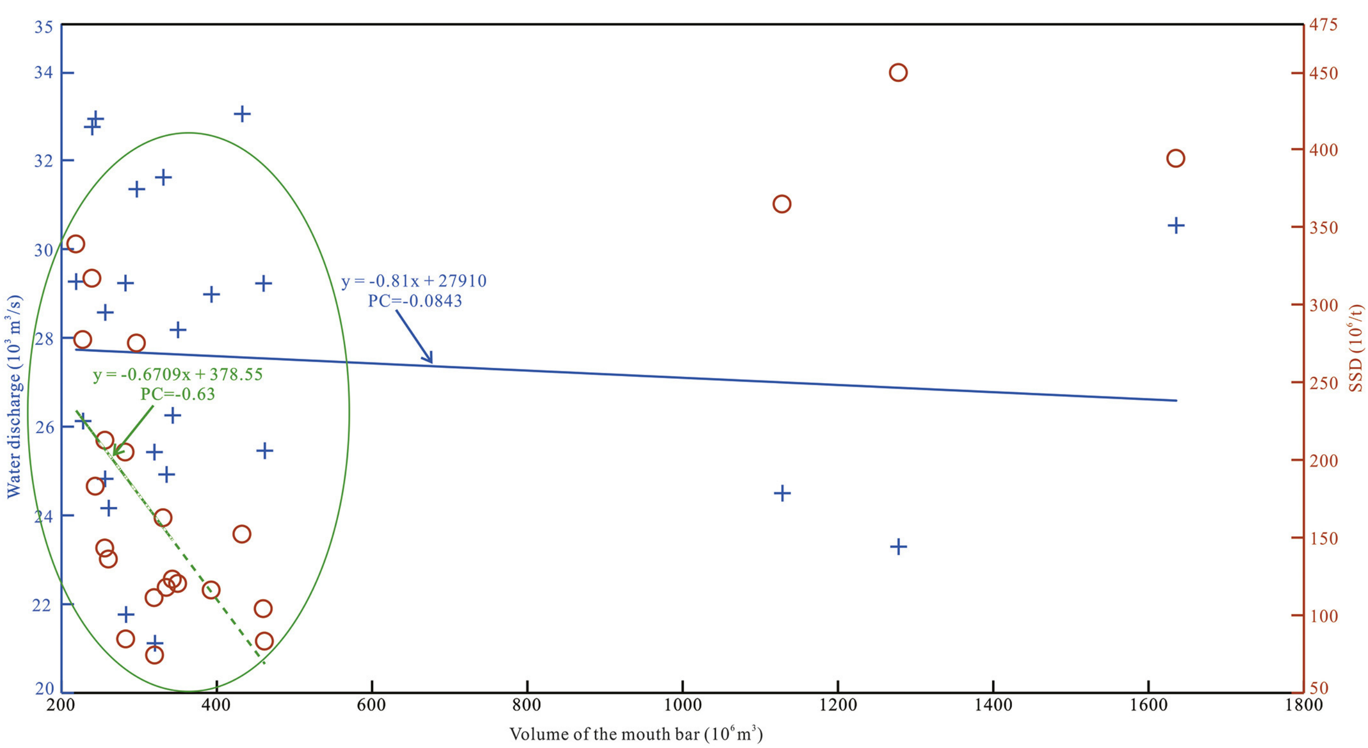

Fig. 9. (a) Correlation analysis between the volume of the inner mouth bar and yearly water discharge (blue circles) and mean yearly suspended sediment discharge (orange circles). Pearson Coefficient (PC) was conducted to illustrate the degree of correlation (blue value represented correlation between volume of inner mouth bar and yearly water discharge and green value represented correlation between volume of inner mouth bar and suspended sediment discharge). (For interpretation of the references to colour in this figure legend, the reader is referred to the web version of this article.)

Table 4
Variation trend of the coefficient of ebb flow of the inner mouth bar during 2002– 2015. Black arrow in the table indicate the variation trend compared with the same or similar month of the former year.

Year	2002		2005		2007		2010		2011		2012		2015
Month	Feb.	Aug.	Feb.	Aug.	Jan.	Aug.	Jan.	Aug.	Feb.	Aug.	Feb.	Aug.	Aug.
SP 2 (%)	51	69	↑64	↓66	/	↓60	↓48	↑69	↑57	/	↓55	↓56	/
SP 4 (%)	/	/	/	/	/	63	/		/	↓60.7	/		↓53.4

mouth bar indexes, and significant correlations inferred that strong ENSO events were responsible for extreme changes in the mouth bar.

Ninety percent and 10% of the ENSO index were set as the thresholds for strong ENSO signals, which were observed in 1974, 1975, 1983, 1989, 1999, 2008, 2010, 2011 and 2016, in which 1974, 1983, 1998, 2010 and 2016 were warm (El Niño) phases, leading to serious floods in the Changjiang basin, and the others were cold (La Niña) phases (Fig. 9). Compared with previously processed topographical data, the mouth bars in these years responded to almost every event. Fig. 11 (green circles) shows that cold events made the volume (b) of the mouth bar shrink in 1989 and clearly moved the top in the upstream direction in 1989, 2008, 2011. However, La Niña events tended to deepen the top and deposited sediment on the landside in 1989, 1999, 2008 and 2011. The opposite change pattern in 1999 may be caused by the effect of extreme floods in 1998. In contrast, in El Niño years (red circles), the volume and landward slope of the mouth bar both decreased (Fig. 10b and e). Particularly for crest distances from the starting point in the flood season, almost every drastic change was related to corresponding ENSO events (Fig. 6c), except in 2006, when an extreme drought occurred (Dai et al., 2011) and a strong tidal force pushed the crest upstream.

4.4. Impact of estuarine engineering projects

Anthropogenic activities always have a significant influence on the geomorphology of an estuary, especially projects that are conducted near mouth bars (Lafite and Louis, 2001; Wal et al., 2002; Hoeksema, 2007; Syvitski et al., 2009; Brunier et al., 2014). In the study area, the diversion ratio in the SP was significantly affected by DWP projects, mostly after 1998 (Liu et al., 2005). Among these 20 years, the first and second stages of the DWP were completed, and the Jiangya North Passage was blocked from 1999–2003 (Fig. 1c), cutting off a flux and suspended sediment transport channel between the NP and SP. Additionally, spur dike construction narrowed the NP, leading to an increasing resistance force, and discharge from the SC tended to flow through the SP. As a result, the diversion ratio of the SP increased in this period. An increasing force from upstream after 1998 resulted in erosion in the upper part of the mouth bar because of a more powerful hydrodynamic force, pushing the crest downstream, and the slope at this side decreased (Figs. 5 and 6).

On the other hand, the diffluence pass project and the construction of levees and groins in the NP created a groove that blocked the Jiangya North Passage, which was a part of the DWP project and caused an increase in the diversion ratio of the SP (Fig. 10a); thus, the IMB's volume and landward slope related to the diversion ratio showed R value of 0.45 and 0.45, respectively (Fig. 10b and d). Comparatively speaking, the crest's elevation and seaward slope generated the R value of 0.34 and 0.31, respectively against the diversion ratio, inferring both the bar's volume and the landward slope had better response to the diversion ratio.

Other classic mouth bars worldwide were impacted to different extents by estuarine projects, and this tendency is likely to increase in the future with the increase in harbor development (Blum and Roberts, 2009; Kondolf et al., 2014; Anthony et al., 2015; Dai et al., 2016). For instance, large amounts of levee construction have limited the plain transport in the Mississippi River Delta (Blum and Roberts, 2009).

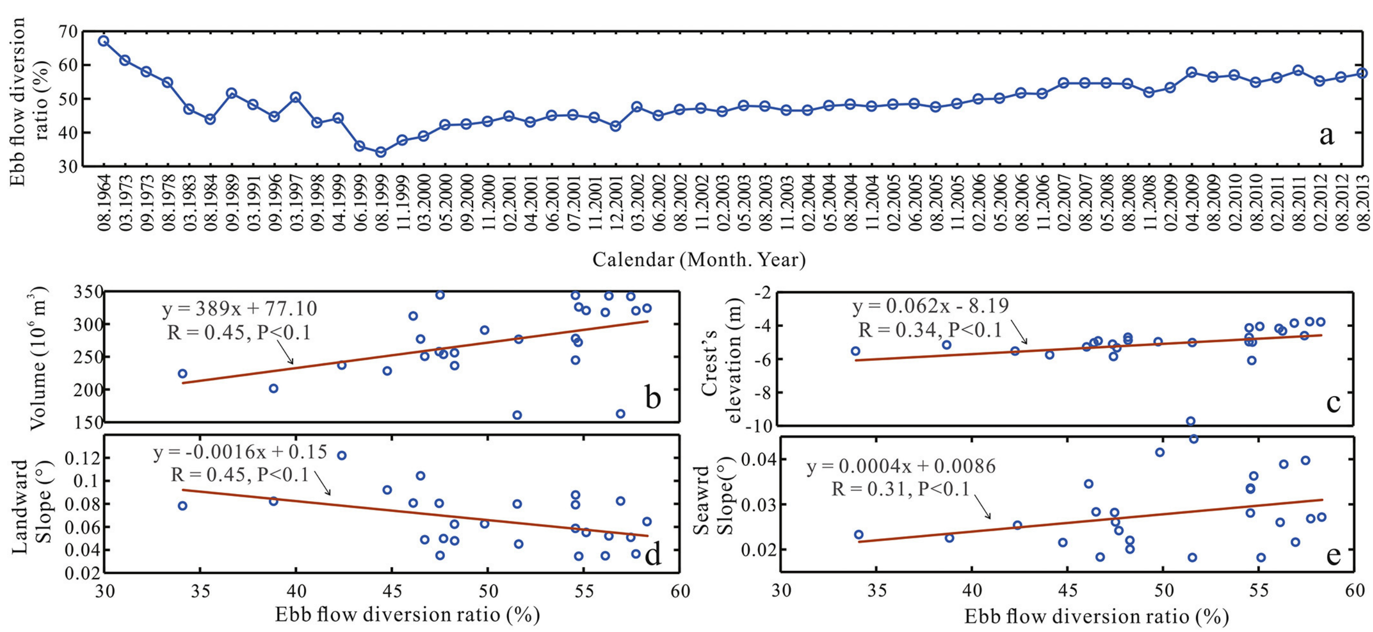

Fig. 10. (a) Ebb flow diversion ratio of the South Passage during 1964–2013; correlation analysis between ebb flow diversion ratio of the South Passage and inner mouth bar's (b) volume; (c) Inner mouth bar's crest elevation; (d), Inner mouth bar's landward slope and (e) inner mouth bar's seaward slope.

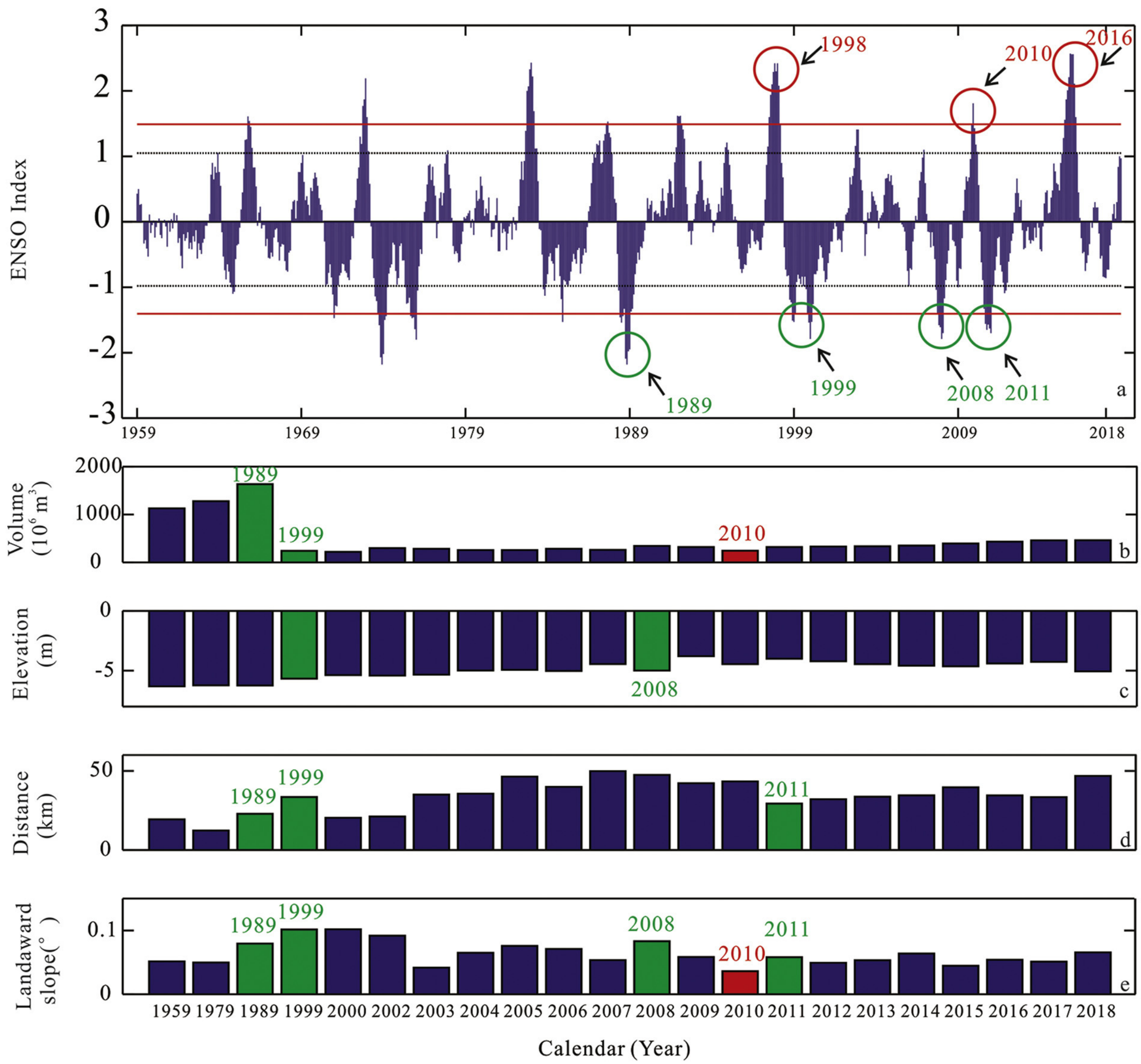

Fig. 11. a) Monthly ENSO index during 1959–2018 period and parameters that responded to the ENSO events with (b) inner mouth bar's volume; (c) inner mouth bar's crest elevation; (d) Distance from the diversion point and (e) inner mouth bar's landward slope.

Although Kondolf et al. (2014) and Anthony (2015) found that the Mekong River Delta suffered rapid erosion because of sediment starvation caused by dam construction, Dai et al. (2016) noticed a different case in the NB of the Changjiang Estuary, in which the reduction in the channel surface area and related tidal prism were mainly affected by local reclamation projects instead of TGD construction upstream.

4.5. Conceptual model of evolution of the inner mouth bar

In this area, complicated factors control the evolution of the mouth bar in the SP, revealing several distinct patterns, which can be classified into the growing phase, partial adjustment phase and stable phase (Fig. 13). Between 1959 and 1979, when the mouth bar in the SP was initially formed and remained in a natural state, the whole body was located in relatively shallow water and was growing with sufficient sediment supply, with an average sediment supply of 466.07 t, which was higher than the nearly 75% sediment supply from 1959 to 2018 (Fig. 3d). A larger diversion ratio brought more sediment to this area, and the mouth bar had not yet been eroded due to the lack of engineering projects, which is one reason why the bar had a large volume. On the other hand, extreme floods caused two cut-offs in the Liuhe Spit (Fig. 1b) in 1958 and 1963, leading to approximately 4 × 10^8 m^3 of sediment moving through the SC-SP route, reaching the SP in 1963 and finally the East China Sea. Therefore, since 1958, this large sediment body had an increasing effect on the mouth bar in the SP (Shen et al., 1983).

In the second stage (Fig. 13 b and c), partial adjustments were made to adapt to the proximal changes. During 1989–1999, an El Niño event occurred (Fig. 10a), which caused an extreme flood in the Changjiang basin, shaving off the crest of the mouth bar and leading to a flat shape with a single crest. Compared to 1989, increased sediment load was supplied upstream (Fig. 3d) in 1999, so its length increased. At the same time, a flood channel appeared, suggesting that tidal forcing had participated in modifying the mouth bar (Fig. 13b).

At the final stage of becoming stable, the mouth bar did not vary significantly (Fig. 12c–d). From 1999 to 2003, the mouth bar had two tops, and the upper bar was deeper than the downstream bar. The landward slope decreased, yet the seaward slope increased at this time, and the upper top was pushed downstream by a stronger force from upstream because of the increased diversion ratio (Fig. 11a). Between 2003 and 2010, with stronger tidal forcing (Table 4) and extreme ENSO events occurring (Fig. 11a), volume of the IMB kept increasing though

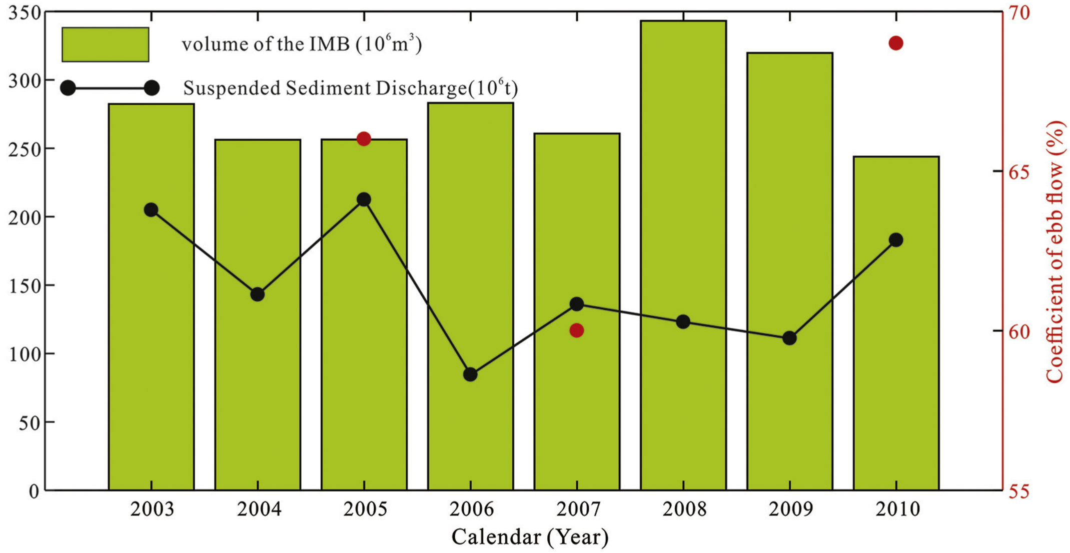

Fig. 12. Variation of volume of the inner mouth bar (green bar), coefficient of the ebb flow (red triangle) and suspended sediment discharge (black line with dots) during 2003 to 2010. (For interpretation of the references to colour in this figure legend, the reader is referred to the web version of this article.)

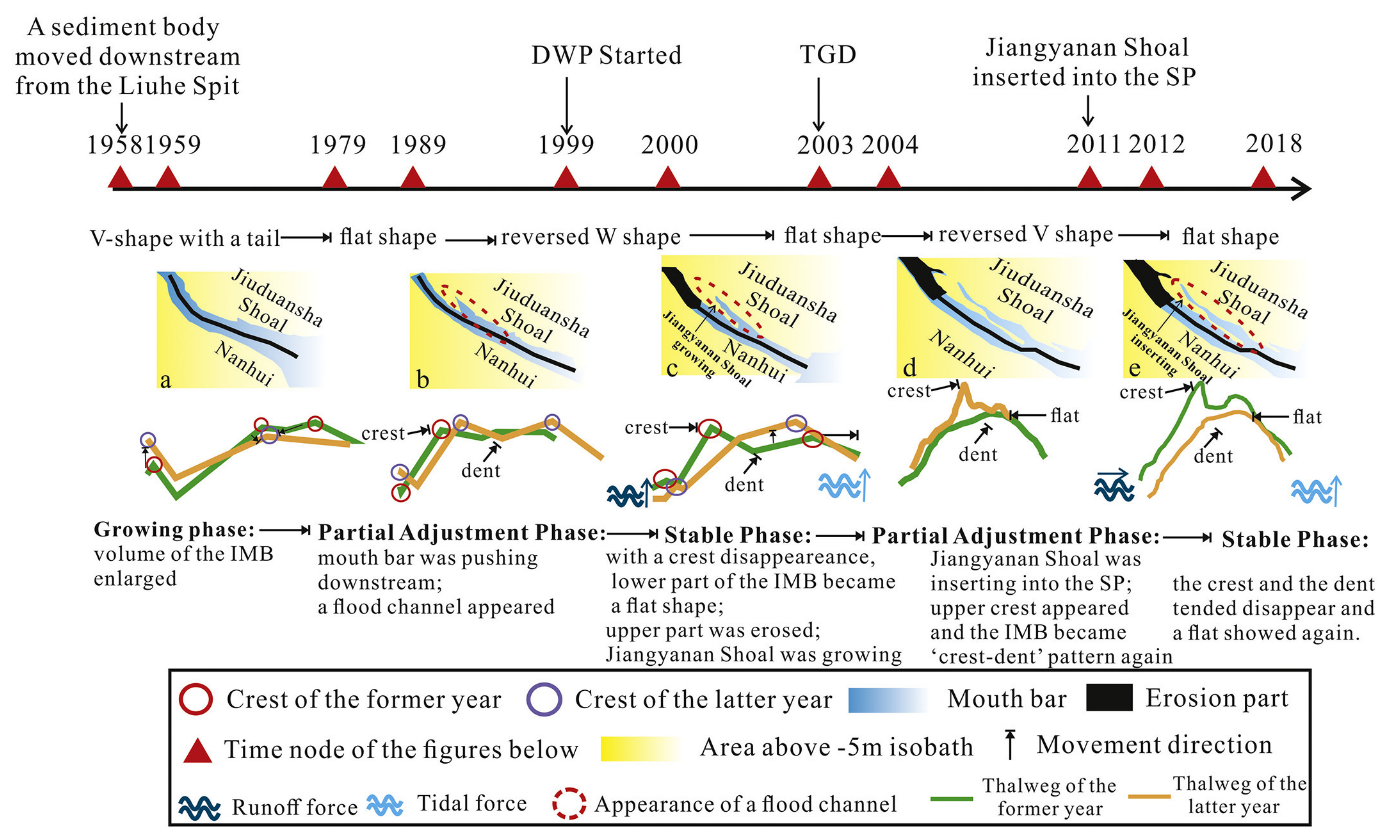

Fig. 13. Conceptual model of evolution of the IMB, when inner mouth bar was at the period of (a) 1959–1979: growing phase; (b) Partial adjustment phase: 1989–1999; (c) Stable phase: 2000–2003; (d) Partial adjustment phase: 2004–2011 and (e) stable phase: 2012–2018.

the SSD from upstream began declining (Fig. 12). Except 2009, the IMB volume during 2005 to 2010 didn't exhibit similar variation trend with the SSD. A decreased ebb flow coefficient in 2007 enlarged the volume of the IMB in 2008. Meanwhile the IMB experienced enlarging and shrinking due to La Niña and El Niño events in 2008 and 2010, respectively (Fig. 11a). Since 2011, the Jiangyanan Shoal enlarged, and its tail moved downstream into the SP (Fig. 13d), which made the flat shape evolved into 'crest-dent' shape again. With a slower development pace of engineering projects after 2011, the stable diversion ratio also helped the mouth bar remain at a stable state landward. Local sandbar's inserting and increasing sediment transportation from seaward made the IMB independent from the fluvial SSD, which also explained the negative correlation between the SSD and the volume of the IMB (Fig. 9).

5. Conclusions

The formation of arcuate IMB in mixed fluvial-tidal estuary channels is of crucial significance, which is directly associated with distributary channel dynamics and deltaic development and is also a major obstacle for commercial shipping and harbor construction (Wright and Coleman, 1974; Anthony, 2015). While previous studies have mainly focused on the shoal mouth bar's evolution process, microcosmic mechanism of mouth bar evolution and the impacts of human activities on changes in mouth bars, our study shows that although the construction of the TGD caused a nearly 70% decline in SSD from upstream (Mei et al., 2018b), the IMB in the SP has continued to increase since 1999 at a rate of 11×10^6 m^3/year. The seasonal characteristics of water discharge are influenced by the TGD; however, the mouth bar remains almost constant throughout the year (Fig. 5). The configuration of the mouth bar showed 5 stages, which were a 'V' shape with a tail (growing phase), and 'crest-dent' shape (partial adjustment phase), and flat shape (stable phase); however, the mouth bar remained arcuate in the longitudinal direction without evident seasonal changes. Although the SSD had a stronger relationship with the volume than water discharge did, they both were not controlling factors of the IMB. Moreover, the tail of the Jiangyanan Shoal moved into the SP and supplied part of the sediment to the mouth bar. On the other hand, the appearance and continuous development of a flood channel in the southern part of the Jiuduansha Shoal suggest increased tidal power from the seaward direction. These coupled impacts formed another sediment source for the mouth bar, preventing it from shrinking. With regard to the SP, where wave had little influence, ENSO events normally were responsible for periodic variations of 2–4 years and are probably the most primary driver of occasional extreme changes to the IMB over a long-term scale. Although the Changjiang basin and estuary have been modified by intensified engineering projects, the long-term evolution and drastic change of the IMB in this basin could be controlled by both natural and anthropogenic forcing, such as diversion project and DWP could disturb this process.

Declaration of Competing Interest

None.

Acknowledgments

This study was supported by the Key projects of intergovernmental science and technology innovation cooperation of the Ministry of Science and Technology in China (2018YFE0109900), International Science and Technology Cooperation Project of Shanghai Science and Technology Commission (19230712400),National Natural Science Foundation of China (NFSC) (41706093), and Fundamental Research Funds for the Central Universities. We thank Wen Wei and Jie Wang for assisting collect data on the SP. Thanks to the three anonymous reviewers' valuable comments, which were much helpful to advance this study.

References

Allison, M.A., 1998. Historical changes in the Ganges-Brahmaputra delta front. J. Coast. Res. 14 (4), 1269–1275.
Andes, L., Cox, A., 2017. Rectilinear inverse distance weighting methodology for bathymetric cross-section interpolation along the Mississippi river. J. Hydrol. Eng. 22 (7), 04017014.
Anthony, E.J., 2015. Wave influence in the construction, shaping and destruction of river deltas: a review. Mar. Geol. 361, 53–78.
Anthony, E.J., Brunier, G., Besset, M., Goichot, M., Dussouillez, P., Nguyen, V.L., 2015. Linking rapid erosion of the Mekong River delta to human activities. Sci. Rep UK 5 (1), 14745.
Blott, S.J., Pye, K., Wal, D.V.D., Neal, A., 2006. Long-term morphological change and its causes in the Mersey estuary, NW England. Geomorphology 81 (1–2), 185–206.
Blum, M.D., Roberts, H.H., 2009. Drowning of the Mississippi delta due to insufficient sediment supply and global sea-level rise. Nat. Geosci. 2 (7), 488–491.
Bonsal, B.R., Zhang, X., Vincent, L.A., Hogg, W.D., 2001. Characteristics of daily and extreme temperatures over Canada. J. Clim. 14 (9), 1959–1976.
Boudet, L., Sabatier, F., Radakovitch, O., 2017. Modelling of sediment transport pattern in the mouth of the Rhone delta: role of storm and flood events. Estuar. Coast. Shelf. S. 198, 568–582.
Brunier, G., Anthony, E.J., Goichot, M., Provansal, M., Dussouillez, P., 2014. Recent morphological changes in the Mekong and Bassac river channels, Mekong delta: the marked impact of river-bed mining and implications for delta destabilisation. Geomorphology 224, 177–191.
Canestrelli, A., Nardin, W., Edmonds, D., Fagherazzi, S., Slingerland, R., 2014. Importance of frictional effects and jet instability on the morphodynamics of river mouth bars and levees. J. Geophys. Res. Oceans 119 (1), 509–522.
Cartwright, D.E., 1974. Years of peak astronomical tides. Nature 248 (5450), 656–657.
Chen, J., Li, D., Chen, B., Hu, F., Zhu, H., Liu, C., 1999. The processes of dynamic sedimentation in the Changjiang estuary. J. Sea Res. 41 (1), 129–140.
Chen, Z., Yu, L., Gupta, A., 2001. The Yangtze river: an introduction. Geomorphology 41 (2), 73–75.
Cuvilliez, A., Deloffre, J., Lafite, R., Bessineton, C., 2009. Morphological responses of an estuarine intertidal mudflat to constructions since 1978 to 2005: the Seine estuary (France). Geomorphology 104 (3–4), 165–174.
Dai, Z., Chu, A., Stive, M., Zhang, X., Yan, H., 2011. Unusual salinity conditions in the Yangtze estuary in 2006: impacts of an extreme drought or of the three Gorges Dam? AMBIO 40 (5), 496–505.
Dai, Z., Liu, J.T., Fu, G., Xie, H., 2013. A thirteen-year record of bathymetric changes in the North passage, Changjiang (Yangtze) estuary. Geomorphology 187, 101–107.
Dai, Z., Fagherazzi, S., Mei, X., Chen, J., Meng, Y., 2016. Linking the infilling of the North branch in the Changjiang (Yangtze) estuary to anthropogenic activities from 1958 to 2013. Mar. Geol. 379, 1–12.
Dai, Z., Du, J., Tang, Z., Ou, S., Brody, S., Mei, X., Jing, J., Yu, S., 2019. Detection of linkage between solar and lunar cycles and runoff of the world's large rivers. Earth Space Sci. 6 (6), 914–930.
Edmonds, D.A., Slingerl, R.L., 2007. Mechanics of river mouth bar formation: implications for the morphodynamics of delta distributary networks. J. Geophys. Res. Earth 112 (2), F02034.
Esposito, C.R., Georgiou, I.Y., Kolker, A.S., 2013. Hydrodynamic and geomorphic controls on mouth bar evolution. Geophys. Res. Lett. 40 (8), 1540–1545.
Falcão, A.P., Mazzolari, A., Gonçalves, A.B., Araújo, M.A.V.C., Trigo-Teixeira, A., 2013. Influence of elevation modelling on hydrodynamic simulations of a tidally-dominated estuary. J. Hydrol. 497, 152–164.
Frihy, O., Lawrence, D., 2004. Evolution of the modern Nile delta promontories: development of accretional features during shoreline retreat. Environ. Geol. 46 (6–7), 914–931.
Gugliotta, M., Saito, Y., 2019. Matching trends in channel width, sinuosity, and depth along the fluvial to marine transition zone of tide-dominated river deltas: the need for a revision of depositional and hydraulic models. Earth Sci. Rev. 191, 93–113.
Haigh, I.D., Eliot, M., Pattiaratchi, C., 2011. Global influences of the 18.6 year nodal cycle and 8.85 year cycle of lunar perigee o high tidal levels. J. Geophys. Res. Oceans 116, C06025.
Hoeksema, R.J., 2007. Three stages in the history of land reclamation in the Netherlands. 56 (Supplement 1), 113–126.
Hoitink, A.J.F., Wang, Z.B., Vermeulen, B., Huismans, Y., Kastner, K., 2017. Tidal controls on river delta morphology. Nat. Geosci. 10 (9), 637–645.
Hu, Z., Yao, P., Van Der Wal, D., Bouma, T.J., 2017. Patterns and drivers of daily bed-level dynamics on two tidal flats with contrasting wave exposure. Sci. Rep UK 7 (1), 7088–7089.
Jaffe, B.E., Smith, R.E., Foxgrover, A.C., 2007. Anthropogenic influence on sedimentation and intertidal mudflat change in San Pablo Bay, California: 1856–1983. Estuar. Coast. Shelf. S. 73 (1–2), 175–187.
Ji-Yu, Chen, Zhu, Shu-Zheng, Quan-Rong, Lü, Yueqin, Zhou, He, Songlin, 1982. Descriptions of the morphology and sedimentary structures of the river mouth bar in the Changjiang estuary. Estuar. Comparisons 667–675.
Kondolf, G.M., Rubin, Z.K., Minear, J.T., 2014. Dams on the Mekong: cumulative sediment starvation. Water Resour. Res. 50 (6), 5158–5169.
Lafite, R., Louis, Alexandre Romaña, 2001. A man-altered macrotidal estuary: the Seine estuary (France): introduction to the special issue. Estuaries. 24 (6), 939.
Leonardi, N., Canestrelli, A., Sun, T., Fagherazzi, S., 2013. Effect of tides on mouth bar morphology and hydrodynamics. J. Geophys. Res. Oceans 118 (9), 4169–4183.
Liu, J., Chen, J.Y., Le, J.H., Huang, R.Y., 2005. Effect of the implementation of the first-stage project of the deep water channel regulation in the Yangtze river estuary on the erosion and deposition in the South passage. J. Sediment. Res. 2005 (5), 40–44.
Liu, J.P., DeMaster, D.J., Nguyen, T.T., Saito, Y., Nguyen, V.L., Ta, Thi Kim Oanh, Li, X., 2017. Stratigraphic formation of the Mekong river delta and its recent shoreline changes. Oceanography 30 (3), 72–83.
Luan, H.L., Ding, P.X., Wang, Z.B., Yang, S.L., Lu, J.Y., 2018. Morphodynamic impacts of large-scale engineering projects in the Yangtze river delta. Coast. Eng. 141 (11), 1–11.
Mei, X.F., Dai, Z.J., Darby, S.E., Gao, S., Wang, J., Jiang, W., 2018a. Modulation of extreme flood levels by impoundment significantly offset by floodplain loss downstream of the three Gorges dam. Geophys. Res. Lett. 45 (7), 3147–3155.
Mei, X.F., Dai, Z.J., Wei, W., Li, W., Wang, J., Sheng, H., 2018b. Secular bathymetric variations of the North channel in the Changjiang (Yangtze) estuary, China, 1880–2013: causes and effects. Geomorphology 303, 30–40.
Milliman, J.D., Huang, T.S., Zuo, S.Y.H., Mead, R., 1985. Transport and deposition of river sediment in the Changjiang estuary and adjacent continental shelf. Cont. Shelf Res. 4 (1–2), 37–45.
Moore, W.S., 1999. The subterranean estuary: a reaction zone of ground water and sea water. Mar. Chem. 65 (1–2), 111–125.
Nardin, W., Fagherazzi, S., 2012. The effect of wind waves on the development of river mouth bars. Geophys. Res. Lett. 39 (12), L12607.
Nardin, W., Mariotti, G., Edmonds, D.A., Guercio, R., Fagherazzi, S., 2013. Growth of river mouth bars in sheltered bays in the presence of frontal waves. J. Geophys. Res.

Earth 118 (2), 872–886.
Nicholls, R.J., Tol, R.S.J., 2006. Impacts and responses to sea-level rise: a global analysis of the SRES scenarios over the twenty-first century. Philos. T. R. Soc. A. 364 (1841), 1073–1095.
Qian, N., Wan, Z.H., 1983. Sediment Dynamics. Science Press, Beijing.
Rahman, A.F., Dragoni, D., El-Masri, B., 2011. Response of the Sundarbans coastline to sea level rise and decreased sediment flow: a remote sensing assessment. Remote Sens. Environ. 115 (12), 3121–3128.
Reeve, D.E., Karunarathna, H., 2009. On the prediction of long-term morphodynamic response of estuarine systems to sea level rise and human interference. Cont. Shelf Res. 29 (7), 938–950.
Robinson, A.H.W., 1960. Ebb-flood channel systems in sandy bays and estuaries. Geography 45 (3), 183–199.
Sabatier, F., Maillet, G., Provansal, M., Fleury, T., Suanez, S., Vella, C., 2006. Sediment budget of the Rhône delta shoreface since the middle of the 19th century. Mar. Geol. 234 (1), 143–157.
Sabatier, F., Samat, O., Ullmann, A., Suanez, S., 2009. Connecting large-scale coastal behaviour with coastal management of the Rhône delta. Geomorphology 107 (1), 79–89.
Sanchez-Arcilla, A., Jimenez, J.A., Valdemoro, H.I., 1998. The Ebro delta: morphodynamics and vulnerability. J. Coast. Res. 14 (3), 754–772.
Shen, J.S., Zhu, Z.M., Zhang, X.Q., 1983. Origin and evolution of the entrance sandbars in the South passage of the Changjiang river estuary. Oceanologia Limnol. Sin. 14 (6), 582–590.
Simmons, H.B., 1955. Some effects of upland discharge on estuarine hydraulics. Proc. ASCE 81, 792.
Swenson, J.B., Paola, C., Pratson, L., Voller, V.R., Murray, A.B., 2005. Fluvial and marine controls on combined subaerial and subaqueous delta progradation: morphodynamic modeling of compound-clinoform development. J. Geophys. Res. 110, 1–16.
Syvitski, J.P.M., Kettner, A.J., Overeem, I., Hutton, E.W.H., Hannon, M.T., Brakenridge, G.R., Day, J., Vörösmarty, C., Saito, Y., Giosan, L., Nicholls, R.J., 2009. Sinking deltas due to human activities. Nat. Geosci. 2 (10), 681–686.
Torrence, C., Compo, G.P., 1998. A practical guide to wavelet analysis. Bull. Am. Meteorol. Soc. 79 (1), 61–78.
Wal, D.V.D., Pye, K., Neal, A., 2002. Long-term morphological change in the Ribble estuary, Northwest England. Mar. Geol. 189 (3), 249–266.
Wei, W., Dai, Z., Mei, X., Gao, S., Liu, J.P., 2019. Multi-decadal morpho-sedimentary dynamics of the largest Changjiang estuarine marginal shoal: causes and implications. Land Degrad. Dev. 30 (17), 2048–2063.
Wilson, C.A., Goodbred Jr., S.L., 2015. Construction and maintenance of the Ganges-Brahmaputra-Meghna delta: linking process, morphology, and stratigraphy. Annu. Rev. Mar. Sci. 7, 67–88.
Wood, F.J., 2001. Tidal dynamics, volume I: theory and analysis of tidal forces. J. Coast. Res. 23 (1), 281.
Wright, L.D., Coleman, J.M., 1974. Mississippi river mouth processes: effluent dynamics and morphologic development. J. Geol. 82 (6), 751–778.
Yang, S., Ding, P., Chen, S., 2001. Temporal change in bed level of a river mouth channel, Yangtze river mouth: with emphasis on the response to river discharge and storm. J. Coast. Res. 17 (2), 297–308.
Yang, S.L., Zhang, J., Zhu, J., Smith, J.P., Dai, S.B., Gao, A., Li, P., 2005. Impact of dams on Yangtze river sediment supply to the sea and delta intertidal wetland response. J. Geophys. Res. Earth 110 (3), F03006.
Zamora, H.A., Nelson, S.M., Flessa, K.W., Nomura, R., 2013. Post-dam sediment dynamics and processes in the Colorado river estuary: implication for habitat restoration. Ecol. Eng. 59, 134–143.
Zhu, B., Li, Y., Yue, Y., Yang, Y., Liang, E., Zhang, C., Borthwick, A., 2020. Alternate erosion and deposition in the Yangtze estuary and the future change. J. Geogr. Sci. 30 (1), 145–163.
Zhu, N., Xu, J., Li, K., Luo, Y., Yang, D., Zhou, C., 2019b. Spatiotemporal change of plum rains in the Yangtze river delta and its relation with EASM, ENSO, and PDO during the period of 1960–2012. Atmosphere 10 (5), 258–277.